Earth Planet. Sci. Lett. 625 (2024) 118489

Contents lists available at ScienceDirect

Earth and Planetary Science Letters

journal homepage: www.elsevier.com/locate/epsl

Calcium isotopes track volatile components in the mantle sources of alkaline rocks and associated carbonatites

Chunfei Chen [a,b,*], Stephen F. Foley [a], Sebastian Tappe [c], Huange Ren [b], Lanping Feng [b], Yongsheng Liu [b,*]

[a] School of Natural Sciences, Macquarie University, North Ryde, New South Wales, 2109, Australia
[b] State Key Laboratory of Geological Processes and Mineral Resources, School of Earth Sciences, China University of Geosciences, Wuhan, 430074, China
[c] Department of Geosciences, UiT - The Arctic University of Norway, N-9037, Tromsø, Norway

ARTICLE INFO

Editor: Dr R. Hickey-Vargas

Keywords:
Ca isotopes
Volatiles
Alkaline rocks
Carbonate
K-richterite
Carbonatites

ABSTRACT

The volatile components CO_2 and H_2O induce mantle melting and thus exert major controls on mantle heterogeneity. Primitive intraplate alkaline magmatic rocks are the closest analogues for incipient mantle melts and provide the most direct method to assess such mantle heterogeneity. Given the considerable Ca isotope differences among carbonate, clinopyroxene, garnet, and orthopyroxene in the mantle (up to 1 ‰ for $\delta^{44/40}$Ca), $\delta^{44/40}$Ca of alkaline rocks is a promising tracer of lithological heterogeneity. We present stable Ca isotope data for ca. 1.4 Ga lamproites, 590–555 Ma ultramafic lamprophyres and carbonatites, and 142 Ma nephelinites from Aillik Bay in Labrador, eastern Canada. These primitive alkaline rock suites are the products of three stages of magmatism that accompanied lithospheric thinning and rifting of the North Atlantic craton. The three discrete magmatic events formed by melting of different lithologies in a metasomatized lithospheric mantle column at various depths: (1) MARID-like components (mica-amphibole-rutile-ilmenite-diopside) in the source of the lamproites; (2) phlogopite-carbonate veins were an additional source component for ultramafic lamprophyres during the second event; and (3) wehrlites at shallower depths were an important source component for nephelinites during the final event.

The Mesoproterozoic lamproites show lower $\delta^{44/40}$Ca values (0.58 to 0.66 ‰) than MORBs (0.84 ± 0.03 ‰, 2se). This cannot be explained by fractional crystallization or melting of the clinopyroxene-dominated source but can be attributed to a source enriched in the alkali amphibole K-richterite, which has characteristically low $\delta^{44/40}$Ca. The $\delta^{44/40}$Ca values of the ultramafic lamprophyre suite during the second rifting stage are remarkably uniform, with overlapping ranges for primary carbonated silicate melts (aillikite: 0.67 to 0.75 ‰), conjugate carbonatitic liquids (0.71 to 0.82 ‰) and silicate-dominated damtjernite liquid (primary damtjernite: 0.68 to 0.72 ‰). This suggests negligible Ca isotope fractionation during liquid immiscibility of carbonate-bearing magmas. Combined with previously reported $\delta^{44/40}$Ca values for carbonatites and kimberlites, our data suggest that carbonated silicate melts in Earth's mantle have $\delta^{44/40}$Ca compositions resolvably lower than those for MORBs (0.74 ± 0.02 ‰ versus 0.84 ± 0.03 ‰, 2se). The $\delta^{44/40}$Ca values of the Cretaceous nephelinites (0.72 to 0.78 ‰) are homogenous and similar to those of the 590–555 Ma ultramafic lamprophyres, suggesting that the wehrlitic source component for the nephelinites formed by mantle metasomatism during interaction with rising aillikite magmas during the second rifting stage. Our results highlight that both K-richterite and carbonate components in mantle sources can result in the systematically low $\delta^{44/40}$Ca values of alkaline magmas, which may explain previously reported low $\delta^{44/40}$Ca values of alkaline rocks and some carbonatites. Our study indicates that Ca isotopes are a robust tracer of lithological variation caused by volatiles in the Earth's upper mantle.

1. Introduction

Lithological and geochemical heterogeneity in Earth's mantle archives mantle evolution, including mantle melting and recycling of crustal materials caused by plate tectonics. Besides pressure and temperature, CO_2 and H_2O contents are the two most important controls on

* Corresponding authors.
E-mail addresses: chfchen2016@hotmail.com (C. Chen), yshliu@hotmail.com (Y. Liu).

https://doi.org/10.1016/j.epsl.2023.118489
Received 19 May 2023; Received in revised form 25 October 2023; Accepted 2 November 2023
Available online 16 November 2023

mantle melting because they cause a significant reduction in the solidus of mantle rocks and a large expansion in the compositional range of melts (Dasgupta, 2018; Foley et al., 2009; Stagno and Frost, 2010), especially at depths greater than 140 km, where melting occurs only when promoted by volatiles (Dasgupta and Hirschmann, 2006; Foley and Pintér, 2018). The volatile-bearing melts produced solidify elsewhere to cause mineralogical and geochemical variations in the Earth's mantle (Aiuppa et al., 2021; Gaillard et al., 2008). It is increasingly recognized that volatile-rich dykes/veins or domains (carbonate, phlogopite, amphibole, and/or fluid) co-exist in the mantle together with the dominant lithology peridotite (Dawson and Smith, 1977; Foley, 1992; Grégoire et al., 2002; Smart et al., 2019; Tappe et al., 2008). Geochemically, volatile-bearing mantle is enriched in fusible components (e.g., K, Na, Ca). Alkaline igneous rocks are generally formed by volatile-triggered mantle melting and hold key information about the role that volatile evolution plays in governing the spatial and temporal variation in mantle rocks, as revealed by major and trace elements, radiogenic isotopes (e.g., Sr, Nd, Hf and Pb isotopes), and olivine geochemistry (Foley et al., 2013; Tappe et al., 2006, 2007).

Stable calcium isotopes ($\delta^{44/40}Ca = (((^{44}Ca/^{40}Ca)_{SAMPLE}/(^{44}Ca/^{40}Ca)_{SRM915a} - 1) \times 1000$) can be used to trace large-scale geological processes, opening a new window in our understanding of alkaline magma origins, including magma processes and the lithology of mantle sources (Antonelli et al., 2023; Eriksen and Jacobsen, 2022; Wang et al., 2019). Considerable equilibrium Ca isotope fractionation (up to 1 ‰) has been observed between the mantle minerals carbonate, clinopyroxene (Cpx), K-richterite, garnet (Grt), and orthopyroxene (Opx) (Antonelli et al., 2019; Chen et al., 2019, 2020b; Xiao et al., 2022): carbonate and hydrous K-richterite have lower $\delta^{44/40}Ca$ values than Cpx. Such inter-mineral Ca isotope differences may result in: (1) large Ca isotope fractionation between melts and residual solids during partial melting (Antonelli et al., 2021; Eriksen and Jacobsen, 2022; Wang et al., 2019); and (2) significant Ca isotope differences between different mantle lithologies, as known for example from the high Ca isotope values for dunite and orthopyroxenite (1.11–1.81 ‰ and 1.13 ‰ $\delta^{44/40}Ca$, respectively) (Chen et al., 2019) and low $\delta^{44/40}Ca$ values for carbonated peridotites (0.56–0.95 ‰, Ionov et al., 2019; Zhu et al., 2021). Therefore, Ca isotopes are potentially a powerful tool for tracing lithological variations caused by volatiles in the mantle sources of alkaline magmas.

The calcium isotope fractionation factor between Cpx and silicate melt is close to 1 (Chen et al., 2019; Zhang et al., 2018), so that $\delta^{44/40}Ca$ values of mid-ocean ridge basalts (MORBs: 0.84 ± 0.03 ‰, 2se) are similar to those of Cpx in spinel peridotites. Recently, Eriksen and Jacobsen (2022) emphasized that melting of a garnet-rich source may result in the light Ca isotope compositions shown by some oceanic island basalts (OIBs) due to the heavier Ca isotope compositions of Grt compared with Cpx (Chen et al., 2020b; Li et al., 2022; Wang et al., 2019). However, possible Ca isotope fractionation in alkaline magmas caused by volatile-bearing minerals or melts in their mantle sources is largely unexplored. Calcium is abundant in several volatile-bearing minerals (e.g., carbonate and richteritic amphiboles) and mantle-derived melts (e.g., carbonatites), and Ca isotope differences between Cpx and volatile-bearing minerals are significant (Wang et al., 2017a; Xiao et al., 2022). Knowledge of Ca isotope fractionation related to the action of volatiles in the mantle is therefore important for understanding the large observed Ca isotope variations and thus the origin of volatile-rich igneous rocks such as silica-undersaturated alkaline

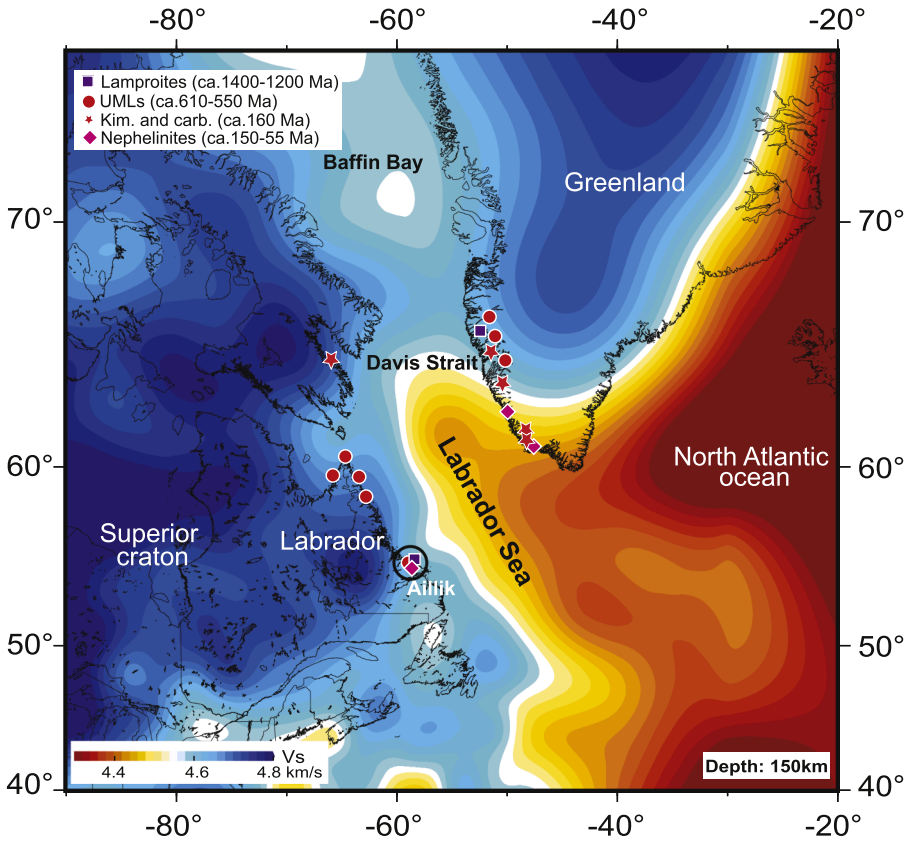

Fig. 1. The locations of alkaline rocks at the flanks of the rift and seismic shear wave velocities beneath the North Atlantic craton and the Labrador Sea at the depth of 150 km. Seismic tomography is from Yuan et al. (2014). The lithosphere beneath Greenland and Labrador shows high velocities similar to the Superior craton, indicating its cratonic nature. The mantle under the Labrador Sea shows low velocity, indicating rifted lithosphere with a higher-velocity ledge in the Davis Strait between Baffin Bay and the Labrador Sea. The locations of the alkaline rocks (UMLs = Ultramafic Lamprophyres and Kim. and carb. = Kimberlites and carbonatites) are from Tappe et al. (2007) and are distributed along the relatively low-velocity zone at the margins of Greenland and Labrador.

rocks, kimberlites, and carbonatites (Amsellem et al., 2020; Antonelli et al., 2023; Banerjee et al., 2021; Sun et al., 2021).

The North Atlantic craton (NAC) was split by continental rifting, ultimately marked by the opening of the Labrador Sea and Davis Strait with short periods of basaltic oceanic crust formation during the early Cenozoic (Fig. 1). Before this, a sequence of ca. 1.4 Ga lamproites, 590–555 Ma ultramafic lamprophyres, and ca. 142 Ma nephelinites at Aillik Bay on the western Labrador Sea margin record a long history of craton breakup during which lithospheric thinning occurred in three main stages (Tappe et al., 2006, 2007). The passive continental margin of Labrador was unaffected by subduction (Keen et al., 2012), and the rifting processes at each of the three stages resulted largely from intra-plate continental stretching. The trace elements and radiogenic isotope compositions of these rift-related alkaline rocks reveal the important role of volatile-rich metasomatized lithospheric mantle sources without notable contributions from subducted crustal materials (Tappe et al., 2006, 2007). The protracted history of this alkaline rock occurrence makes it an ideal target to explore Ca isotope fractionation induced by volatiles in the upper mantle. We have undertaken a detailed Ca isotope study on the diverse magmatic products of the three rifting stages and our results show how the lithological variations caused by volatiles in Earth's upper mantle may fractionate the Ca isotopes of alkaline and carbonate-rich magmatic rocks.

2. Geological setting and samples

The NAC was split during the Mesozoic-Cenozoic into two continental blocks – the Nain Province of Labrador and the Archaean terranes of West Greenland, separated by the Labrador Sea (Fig. 1). The Archaean blocks on either side of the Labrador Sea preserve tonalitic crust as old as 3.8 Ga and thick cratonic mantle roots persist to the present day (Windley and Garde, 2009). The Archaean cores were augmented by the accretion of micro-continents assembled during the Paleoproterozoic (1.9–1.7 Ga) marking the final phase of cratonization through a sequence of subduction and collision events (Wardle and Hall, 2002). The NAC has experienced numerous mantle-derived alkaline igneous events since the Proterozoic (Larsen and Rex, 1992), which eventually accompanied rifting that proceeded to the production of oceanic crust in the Labrador Sea for a short time interval during the early Cenozoic. The uplifted basement blocks of the NAC record one of the longest craton splitting histories known: the first stage corresponds to impregnation of the mantle lithosphere with K-rich silicate melts >2000 Myr ago, which was reactivated and melted at ca. 1370 Ma to produce olivine lamproite magmas. The second stage is represented by widespread emplacement of ultramafic lamprophyres and carbonatites in the late Neoproterozoic (Fig. 1), and the third episode led to successful rifting and the production of new oceanic crust, preceded by the eruption of kimberlites, ultramafic lamprophyres and carbonatites in western Greenland between ca. 200–150 Ma (Tappe et al., 2017), and eventually nephelinite and melilitite magmas along the rift flanks at ca. 150–100 Ma (Tappe et al., 2006, 2007).

The samples selected for Ca isotopic analysis are from the Aillik Bay locality (Fig. 1), which is the only known area where all three rifting stages are recorded by the occurrence of alkaline magmatic rocks. The samples include four 1.37 Ga old lamproites, 21 ultramafic lamprophyres and carbonatites emplaced between 590 and 555 Ma, and five nephelinites and melilitites dated at ca. 142 Ma. The ultramafic lamprophyres are primitive SiO_2-poor potassic igneous rocks comprising aillikites (for which Aillik Bay is the type locality), mela-aillikites, and damtjernites following the classification of Tappe et al. (2005), in which aillikites are the archetypal carbonate-rich member of the ultramafic lamprophyre group (Malpas et al., 1986; Rock, 1986). Detailed descriptions and age determinations of the rocks analyzed in this study, along with their major and trace element contents and Sr-Nd-Hf-Pb isotopic compositions, can be found in Tappe et al. (2006), Tappe et al. (2007), and Table S1.

3. Analytical methods

Chemical purification and measurement of Ca isotope ratios were performed at the State Key Laboratory of Geological Processes and Mineral Resources, China University of Geosciences, Wuhan, China, with methods following Feng et al. (2018). Briefly, Ca was separated from the sample matrix on micro-columns filled with Ca-selective DGA resin. High recovery (> 99 %), efficient separation of Ca, and a low total procedural blank of <10 ng were achieved. Following purification, calcium isotopic compositions were analyzed on a Neptune Plus (Thermo Scientific, Bremen, Germany) MC-ICP-MS collecting $^{42}Ca^{+}$, $^{43}Ca^{+}$, and $^{44}Ca^{+}$ isotopes using Faraday cups at L3, L2, and central positions, respectively. The signal at m/z 43.5 was also collected at L1 to monitor the doubly charged interference of Sr on Ca isotopes and was found to be negligible for purified samples. Isotope measurements were performed using standard-sample bracketing to correct for instrumental drift and results are defined using δ-notation: $\delta^{42}_{n}Ca = [(^{n}Ca/^{42}Ca)_{sample}/(^{n}Ca/^{42}Ca)_{SRM915a}\text{-}1] \times 1000$ where $n = 44$ or 43. All measured Ca isotope values ($\delta^{44/42}Ca$) were converted to $\delta^{44/40}Ca$ using a factor of 2.048 calculated by the mass-dependent fractionation law (Heuser et al., 2016). The long-term external 2sd reproducibility of 0.08 ‰ for $\delta^{44/40}Ca$ in this study is assessed based on replicate measurements of Alfa Ca over the course of half a year (Fig. S1 in Section 1 of Supplementary Information).

Three reference materials (COQ-1, BHVO-2, and BCR-2) and three duplicate samples were processed as unknowns to assess accuracy and reproducibility. We obtained $\delta^{44/40}Ca$ of 0.74 ± 0.06 ‰ (2sd, $n = 4$), 0.77 ± 0.07 ‰ (2sd, $n = 6$), and 0.83 ± 0.08 ‰ (2sd, $n = 3$) for COQ-1, BHVO-2, and BCR-2, respectively (Fig. S2 and Table 1), consistent with previous studies within the analytical uncertainty (Amini et al., 2009; Amsellem et al., 2017; Feng et al., 2017; He et al., 2017; Schiller et al., 2012; Valdes et al., 2014). Three duplicate samples show good reproducibility within analytical uncertainty (Table 1). Furthermore, Antonelli et al. (2023) showed the generally good agreement on analytical results for the same kimberlite powders between our laboratory and the laboratory at Chengdu University of Technology using the double-spike thermal ionization mass-spectrometry. Measured $\delta^{44/42}Ca$ and $\delta^{43/42}Ca$ of the alkaline rocks and reference materials plot on a line of theoretical kinetic fractionation with a slope of 0.506 within uncertainty (Heuser et al., 2016) (Fig. S3), reflecting mass-dependent fractionation without analytical artifacts from mass spectrometric interferences.

4. Results

Calcium isotopic compositions of the alkaline rocks and carbonatites from Aillik Bay and reference materials are reported in Table 1. Due to the large interference of $^{40}Ar^{+}$ from the argon carrier gas on ^{40}Ca in analytes within the ICP-MS instrument, the $^{44}Ca/^{40}Ca$ ratio could not be determined directly in this study. All $\delta^{44/40}Ca$ values were obtained by conversion of measured $\delta^{44/42}Ca$ applying the mass-dependent fractionation law. Thus, $\delta^{44/40}Ca$ variations in our samples reflect mass-dependent fractionation without the effect of ^{40}Ca ingrowth from the radioactive decay of ^{40}K. We also calculated $\delta^{44/40}Ca$ values accounting for ^{40}Ca addition from the radioactive decay of ^{40}K ($\delta^{44/40}Ca_{Radiogenic}$ in Table 1; for calculation see Fu et al. (2022)); however, in this study we only use the uncorrected $\delta^{44/40}Ca$ values for our samples to discuss the mass-dependent fractionation without the effect of radiogenic excess ^{40}Ca.

The Mesoproterozoic olivine lamproites show a small variation of $\delta^{44/40}Ca$ values from 0.58 to 0.66 ‰, lower than MORB values (0.84 ‰, Chen et al., 2020a; Eriksen and Jacobsen, 2022; Zhu et al., 2018) (Fig. 2). The $\delta^{44/40}Ca$ values of the Late Neoproterozoic ultramafic lamprophyres range from 0.56 to 0.75 ‰ (Fig. 2). Among them, aillikites and mela-aillikites have homogeneous Ca isotopic compositions of 0.67 to 0.75 ‰, also systematically lower than MORB values but higher than the olivine lamproites. The $\delta^{44/40}Ca$ values of the Neoproterozoic

Table 1
Ca–Sr–C–O isotopic compositions and melting temperatures (T) and pressures (P) of the alkaline rocks and associated carbonatites at Aillik Bay and reference materials.

Samples	$\delta^{44/42}$Ca	2sd	$\delta^{43/42}$Ca	2sd	$\delta^{44/40}$Ca[a]	2sd	2se	n	$\delta^{44/40}Ca_{Radiogenic}$[b]	$^{87}Sr/^{86}Sr_i$[c]	δ^{13}C[c]	δ^{18}O[c]	T[d]	P[d]
	‰		‰		‰				‰		‰	‰	°C	GPa
Mesoproterozoic olivine lamproites (1374 Ma)														
ST115a	0.30	0.01	0.16	0.07	0.60	0.03	0.02	3	0.47	0.7048			1429	4.8
ST208	0.28	0.01	0.16	0.03	0.58	0.03	0.02	3	0.43	0.7049			1436	5.1
ST223	0.32	0.01	0.15	0.04	0.66	0.03	0.01	3	0.56	0.7047			1372	4.1
ST237	0.28	0.05	0.14	0.06	0.58	0.11	0.06	3	0.41	0.7056			1514	5.6
Late Neoproterozoic aillikites (590–555 Ma)														
ST164	0.36	0.06	0.19	0.05	0.75	0.13	0.08	3	0.74	0.7039	−5.2	9.4	1426	5.3
ST198a	0.34	0.03	0.18	0.01	0.70	0.05	0.03	3	0.69	0.7037			1502	6.4
ST225	0.35	0.06	0.17	0.04	0.71	0.12	0.07	3	0.71	0.7038			1444	6.2
ST250a	0.35	0.05	0.16	0.10	0.72	0.10	0.06	3	0.71	0.7039	−5.0	11.0	1427	5.0
Late Neoproterozoic mela-aillikites (590–555 Ma)														
ST147b	0.33	0.01	0.15	0.08	0.67	0.03	0.02	3	0.66	0.7038				
ST196	0.35	0.04	0.16	0.10	0.71	0.09	0.05	3	0.70	0.7033				
ST244b	0.35	0.02	0.15	0.02	0.72	0.05	0.03	3	0.71	0.7046				
Late Neoproterozoic damtjernites (590–555 Ma)														
ST140	0.33	0.03	0.15	0.01	0.68	0.05	0.03	3	0.68	0.7036				
ST174	0.28	0.03	0.14	0.04	0.56	0.07	0.04	3	0.56	0.7040				
ST188a	0.34	0.02	0.19	0.06	0.70	0.05	0.03	3	0.69	0.7036	−7.0	11.4		
ST206a	0.29	0.05	0.15	0.10	0.60	0.11	0.06	3	0.59	0.7038	−4.7	9.9		
ST224b	0.35	0.07	0.15	0.13	0.72	0.14	0.08	3	0.72	0.7040				
ST226	0.31	0.03	0.15	0.06	0.62	0.11	0.07	3	0.62	0.7039	−5.9	10.4		
ST114	0.34	0.07	0.16	0.02	0.70	0.13	0.08	3	0.69					
ST170	0.29	0.01	0.14	0.02	0.59	0.14	0.08	3	0.59					
Replicate	0.32	0.03	0.18	0.06	0.65	0.03	0.02	3						
ST256	0.35	0.04	0.19	0.01	0.71	0.07	0.04	3	0.70	0.7050				
Late Neoproterozoic carbonatites (590–555 Ma)														
ST203	0.44	0.03	0.23	0.06	0.90	0.06	0.03	3	0.90	0.7047	−2.8	10.8		
ST126	0.40	0.02	0.19	0.07	0.82	0.03	0.02	3	0.82	0.7058	−3.3	10.2		
ST193a	0.35	0.03	0.20	0.02	0.71	0.06	0.04	3	0.71	0.7039				
Replicate	0.35	0.01	0.16	0.06	0.71	0.03	0.02	3						
ST198c	0.35	0.03	0.17	0.07	0.71	0.06	0.03	3	0.71	0.7039	−3.7	10.8		
ST199	0.37	0.04	0.16	0.04	0.76	0.07	0.04	3	0.76	0.7039	−4.8	10.0		
Cretaceous nephelinites (141 Ma)														
ST100	0.38	0.03	0.20	0.03	0.78	0.05	0.03	3	0.78	0.7047			1252	2.5
ST102	0.35	0.03	0.17	0.03	0.72	0.06	0.03	3	0.72	0.7049			1288	2.7
ST103	0.36	0.03	0.16	0.07	0.74	0.04	0.02	3	0.74	0.7062			1309	2.8
Replicate	0.38	0.01	0.17	0.07	0.77	0.06	0.03	3						
ST253	0.37	0.03	0.17	0.06	0.76	0.06	0.04	3	0.76	0.7056			1322	2.9
ST254	0.37	0.04	0.18	0.05	0.76	0.09	0.05	3	0.75	0.7052			1270	2.7
Reference materials														
COQ-1	0.36	0.03	0.18	0.06	0.74	0.06	0.04	3						
BHVO-2	0.38	0.04	0.17	0.02	0.77	0.07	0.04	3						
BCR-2	0.40	0.04	0.18	0.07	0.83	0.08	0.05	3						
Replicate	0.39	0.03	0.16	0.05	0.79	0.06	0.03	3						

[a] $\delta^{44/40}$Ca obtained using the mass-dependent fractionation law: $\delta^{44/40}Ca = 2.048 \times \delta^{44/42}Ca$ (Heuser et al., 2016).
[b] $\delta^{44/40}Ca_{Radiogenic}$ is calculated by the addition of ^{40}Ca ingrowth via the decay of ^{40}K to ^{40}Ca, details see Fu et al. (2022).
[c] The Sr isotopes and C–O isotopes of the alkaline and carbonatite rocks are from Tappe et al. (2006) and Tappe et al. (2007).
[d] Estimate based on thermobarometry of silica-undersaturated melts developed by Sun and Dasgupta (2020).

carbonatites are also homogenous (0.71 to 0.82 ‰, except for one carbonatite at 0.90 ‰), consistent with those of aillikites and mela-aillikites. The $\delta^{44/40}$Ca values of the damtjernites show a larger range from 0.56 to 0.72 ‰, with five relatively primitive damtjernites at 0.68–0.72 ‰ and four more evolved damtjernites at 0.56–0.62 ‰ (Fig. 2). The $\delta^{44/40}$Ca values of the Cretaceous nephelinites vary from 0.72 to 0.78 ‰ (Fig. 2), similar to the aillikites and mela-aillikites.

5. Discussion

The calcium isotopic compositions of magmatic rocks may be significantly modified by precipitation of Ca-rich secondary minerals such as hydrothermal carbonates. The lamproite, ultramafic lamprophyre, carbonatite, and nephelinite samples studied here are very fresh with only little or no signs of hydrothermal overprinting: no secondary alteration was observed during petrographic analysis (Tappe et al., 2006, 2007). For magmatic silicate rocks, the lack of correlation between $\delta^{44/40}$Ca values and CO_2 contents in the lamproites and nephelinites indicates a negligible effect of alteration on their Ca isotopic compositions (Fig. S4a). The magmatic carbonate-bearing aillikites and damtjernites have overlapping mantle-like δ^{13}C and δ^{18}O values (Tappe et al., 2006), in contrast to strongly fractionated carbonatites (Fig. S4b). Importantly, the lamproite, aillikite, and nephelinite suites each have homogenous Ca isotope compositions, which suggests that their $\delta^{44/40}$Ca values are unaffected by hydrothermal processes (Fig. 2).

5.1. Mantle source lithologies and melting conditions at Aillik Bay

The fractional crystallization history of the alkaline rocks needs to be assessed before decoding their mantle source lithologies using Ca isotope geochemistry alongside standard petrological tools. The Mesoproterozoic lamproites contain olivine phenocrysts with a small amount of clinopyroxene, phlogopite and apatite, suggesting that they mainly experienced fractional crystallization of olivine (Tappe et al., 2007). Uniform CaO/Al_2O_3 ratios with variation in MgO contents in the lamproites also indicates fractional crystallization of olivine without clinopyroxene (Fig. 3a). This is supported by fractional crystallization modeling of an experimental lamproite melt from Foley et al. (2022)

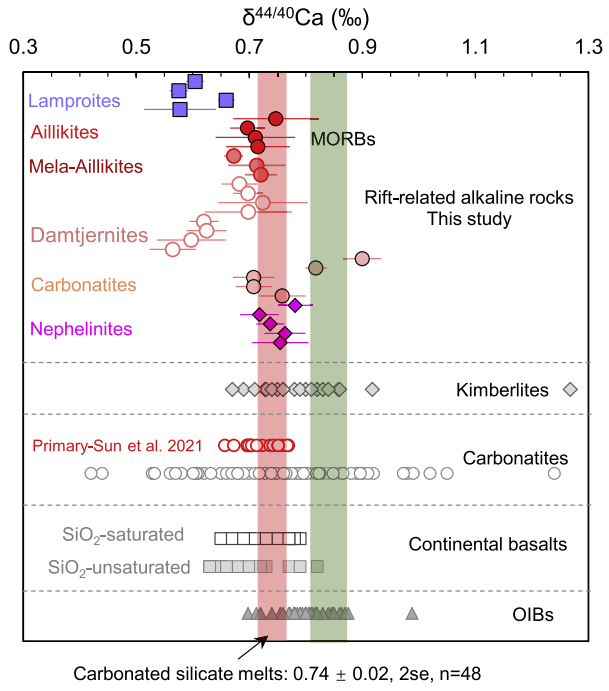

Fig. 2. $\delta^{44/40}$Ca values of the alkaline rocks from Aillik Bay compared to average MORBs (Chen et al., 2020a; Eriksen and Jacobsen, 2022; Zhu et al., 2018), kimberlites (Antonelli et al., 2023; Tappe et al., 2021), carbonatites (Banerjee et al., 2021; Sun et al., 2021), continental silica-saturated basalts (Liu et al., 2017) and silica-unsaturated basalts (Qi et al., 2022; Zhao et al., 2022), and oceanic island basalts (OIBs) in publications since 2015 (Eriksen and Jacobsen, 2022; He et al., 2017; Jacobson et al., 2015; Zhang et al., 2018).

using MELTS (Gualda and Ghiorso, 2015), which shows that fractional crystallization of lamproite melt is dominated by olivine until <3.5 wt.% MgO is reached (Fig. 3a; for modeling parameters see Table S2). The high MgO contents of the olivine lamproites (mostly >8.1 wt.%) indicate that they represent relatively primitive magmas (Tappe et al., 2007). The Mesozoic nephelinites contain olivine and clinopyroxene phenocrysts. The positive correlation between the CaO/Al_2O_3 ratio and MgO content for the nephelinites indicates that they underwent fractional crystallization of both olivine and clinopyroxene, consistent with fractional crystallization modeling of an experimental nephelinite melt from Dasgupta et al. (2007) using MELTS (Gualda and Ghiorso, 2015) (Fig. 3a and Table S2).

The major element compositions of mantle-derived magmas can be used to constrain source lithologies. Low CaO contents and high FC3MS values ($FeO/CaO-3*MgO/SiO_2$) are typical features of basaltic melts derived from pyroxenites (Lambart et al., 2013; Yang et al., 2016). The Mesoproterozoic lamproites have high FC3MS values but low CaO contents (6.3–7.8 wt.%), different from any experimental melts of peridotite but similar to melts of pyroxenite or MARID metasomes (mica-amphibole-rutile-ilmenite-diopside) (Fig. 4). Although fractional crystallization of clinopyroxene could produce high FC3MS values and low CaO contents, these lamproites did not experience clinopyroxene fractionation. The high K_2O contents (5.1–7.7 wt.%) of the lamproites require a source containing K-rich minerals (e.g., phlogopite or potassic richterite). Their EM1-like Sr-Nd-Hf-Pb isotope compositions also fingerprint long-term enriched cratonic mantle components, which can be explained by K-rich ultramafic veins in peridotite (Tappe et al., 2007). Furthermore, the Mesoproterozoic lamproites resemble the experimental melts of MARID assemblages (Foley et al., 2022) and are different from experimental melts of phlogopite clinopyroxenite (Funk and Luth, 2013; Lloyd et al., 1985), supporting a MARID-style metasomatized mantle source (Fig. 4b).

Among the Neoproterozoic ultramafic lamprophyres, primitive aillikites have low SiO_2 and high CaO and MgO contents, similar to experimental melts of carbonated peridotite at ≥3 GPa (Fig. 4a). Their olivine phenocryst geochemistry (Veter et al., 2017) and bulk chemical and isotopic compositions (Tappe et al., 2006, 2007) are consistent with melting of a carbonated mantle source. The Mesozoic nephelinite suite at Aillik Bay comprises dykes and sills of nephelinite and basanite, plus rare melilitite (Tappe et al., 2007). The high MgO (6.9–11.3 wt.%), Ni (76–198 ppm), and Cr contents (123–485 ppm) of this alkaline rock suite indicate derivation from primitive mantle-sourced magmas, and their high CaO contents (10.3–14.6 wt.%) and relatively low FC3MS values are also consistent with experimental melts of peridotite (Fig. 4a). Their low SiO_2 (34.7–44.3 wt.%) contents resemble experimental melts of peridotite in the presence of CO_2 at 2–3 GPa (Green and Falloon, 1998), indicating the involvement of wehrlite in their mantle source (Tappe et al., 2007).

Temperatures and pressures of melt formation are estimated using the method of Sun and Dasgupta (2020), which was calibrated for CO_2-rich, silica-undersaturated magmatic systems. This thermobarometer treats the Mg-number of olivine in the mantle source and the H_2O content of primary magmas as key parameters (Supplementary

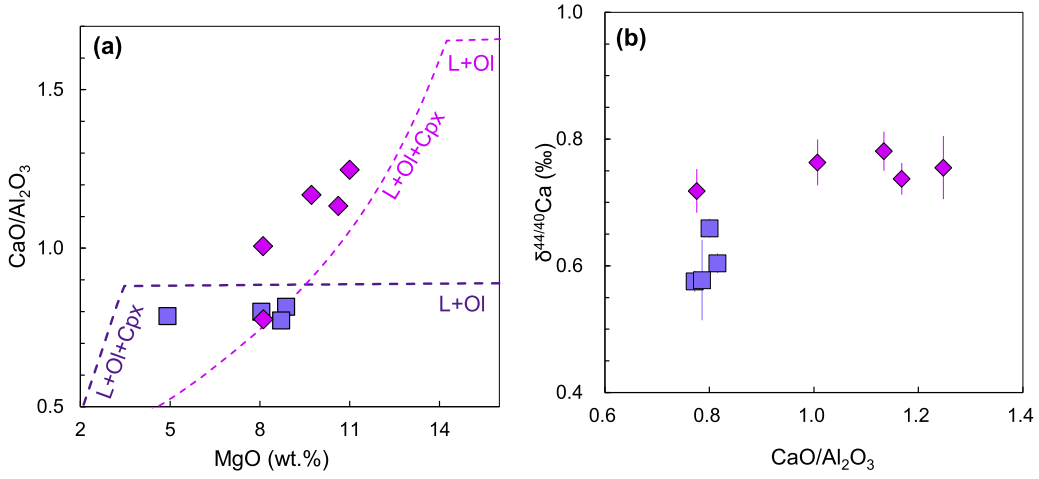

Fig. 3. Bulk rock MgO content versus CaO/Al_2O_3 ratio (a) and $\delta^{44/40}$Ca value versus CaO/Al_2O_3 ratio (b) for Mesoproterozoic lamproites and Cretaceous nephelinites from Aillik Bay. Modeled crystallization of an experimental lamproite melt (blue line) from Foley et al. (2022) and an experimental nephelinite melt (magenta line) from Dasgupta et al. (2007) using MELTS (Gualda and Ghiorso, 2015) are shown for comparison. The phases during crystallization modeling (L-liquid, Ol-olivine, Cpx-clinopyroxene) are shown along the lines.

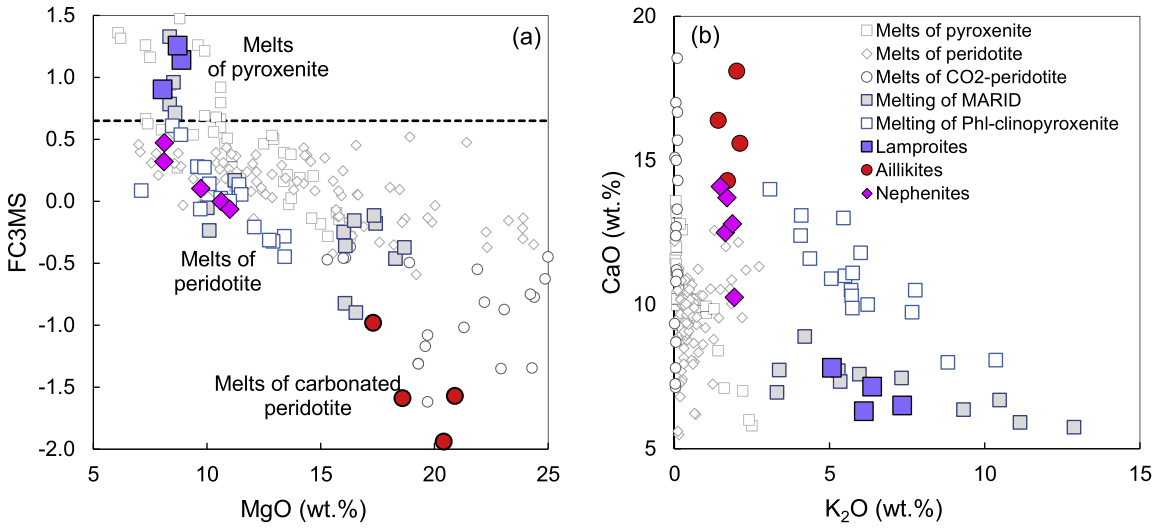

Fig. 4. (a-b) Bulk rock MgO content versus FC3MS (FeO/CaO-3*MgO/SiO_2) and bulk rock K_2O versus CaO content for Mesoproterozoic lamproites, Neoproterozoic ultramafic lamprophyres, and Cretaceous nephelinites from Aillik Bay. Data for experimental pyroxenite melt and peridotite melt were compiled by Yang et al. (2016). In (a), the dotted line indicates the upper boundary for peridotite melts (Yang et al., 2016), discriminating melts from pyroxenite and peridotite. Experimental melts of MARID (Foley et al., 2022) and phlogopite clinopyroxenites (Funk and Luth, 2013; Lloyd et al., 1985) are also shown for comparison.

Information). The results in Fig. S5 and Table 1 indicate melting pressures of approximately 4–6 GPa for both lamproites and aillikites, and 2–3 GPa for the nephelinites, broadly consistent with the petrogenetic model for the evolution of alkaline magmatism at Aillik Bay (Tappe et al., 2007). The temperature estimates are approximately 1370–1500 °C for the lamproites and aillikites, and 1250–1360 °C for the nephelinites. To examine the reliability of these temperature models, we calculated the crystallization temperature of nephelinite sample ST103 (~1200 °C) using Al-in-olivine thermometry (Coogan et al., 2014). Given that the nephelinite magma crystallization temperature is ~100 °C lower than the calculated melting temperature of the mantle source, we place confidence in these results. The melting temperatures are higher than the warmest known cratonic geotherms (Lee et al., 2011) and correspond broadly to the thermal regime of the underlying asthenosphere, indicating that melting was initiated by asthenospheric flow.

5.2. Origin of lamproites from K-richterite-bearing metasomes with low $\delta^{44/40}Ca$

Due to the extremely low CaO contents of the olivine phenocrysts (<0.012 wt.% CaO, Tappe et al., 2007), fractional crystallization of olivine changes neither CaO/Al_2O_3 nor $\delta^{44/40}Ca$ of the magma (Fig. 3). Furthermore, the lamproites show homogenous Ca isotopic compositions regardless of variable CaO and MgO contents, demonstrating the limited effect of fractional crystallization on the $\delta^{44/40}Ca$ compositions. Apatite has slightly lower $\delta^{44/40}Ca$ than Cpx (Xiao et al., 2022), so that fractionation of minor apatite would result in slightly heavier Ca isotope compositions of the residual melt, contrasting with the light Ca isotopes of the Mesoproterozoic lamproites. Therefore, the $\delta^{44/40}Ca$ values of the lamproites must reflect the Ca isotopic compositions of their parental magmas.

The Ca isotope compositions of the Mesoproterozoic lamproites are lighter than those of MORBs (Chen et al., 2020a; Eriksen and Jacobsen, 2022; Zhu et al., 2018). This can be attributed to either isotope fractionation during the melting of MARID or inheritance of Ca isotope compositions from the MARID component that already possessed low $\delta^{44/40}Ca$. K-richterite and clinopyroxene are the two major Ca-phases in MARID assemblages. K-richterite is fully consumed in melting reactions within 50 °C of the MARID solidus (Foley et al., 2022), and it has much lower $\delta^{44/40}Ca$ values than Cpx (Xiao et al., 2022). Given that the fractionation factor for Ca isotopes between clinopyroxene and silicate melt is close to 1, K-richterite would have lighter Ca isotopes than its equilibrium silicate melts (Fig. 5a). The $\delta^{44/40}Ca$ values of melts produced from MARID assemblages are higher than the residue and starting material if K-richterite is not completely consumed, and would approach the source values if K-richterite is completely consumed (Fig. 5b, Supplementary information: Section 3.1, and Table S3). Calcium isotope fractionation induced by partial melting cannot explain the light Ca isotopes in the Mesoproterozoic lamproites. We therefore suggest that the K-richterite in the MARID source carried the low $\delta^{44/40}Ca$ signature. The Ca isotope compositions of mantle rocks are also dependent on their mineralogy; for example, dunite and orthopyroxenite have heavy Ca isotopes due to the modal dominance of olivine and Opx, respectively (Chen et al., 2019). Similarly, K-richterite-bearing MARID assemblages would have much lower Ca isotope compositions than peridotites due to the low $\delta^{44/40}Ca$ nature of K-richterite (Xiao et al., 2022).

K-richterite-bearing MARID was formed by reaction of infiltrating hydrous silicate melts with the refractory cratonic mantle lithosphere. Considering the much lower CaO content of refractory harzburgite (<0.5 wt.%, Pearson et al. (2003)) than that of hydrous silicate melt (for example, the average CaO contents of worldwide continental basalts are 7.3–11.1 wt.%, Farmer (2014)), the Ca isotopes in K-richterite-bearing MARID are not affected by the refractory cratonic mantle, but are controlled by metasomatic melts. We modeled the Ca isotope compositions of K-richterite-bearing MARID material formed by mantle metasomatism at the base of the cratonic lithosphere for different geothermal gradients (Fig. 5c). These calculations assume that the hydrous silicate melts that caused the metasomatism had a MORB-like $\delta^{44/40}Ca$ value of 0.84 ‰ (Supplementary Information: Section 3.2). Results show that the K-richterite-bearing MARID has a theoretical $\delta^{44/40}Ca$ value of 0.65 ‰ at 950–1100 °C. This model temperature range provides a realistic analogue to natural MARID assemblage formation by melt/fluid metasomatism in the relatively cold cratonic mantle (Fitzpayne et al., 2018a, 2018b). Therefore, the light Ca isotope compositions of the Mesoproterozoic lamproites from the NAC indicate a mantle source containing K-richterite-bearing MARID-type metasomes.

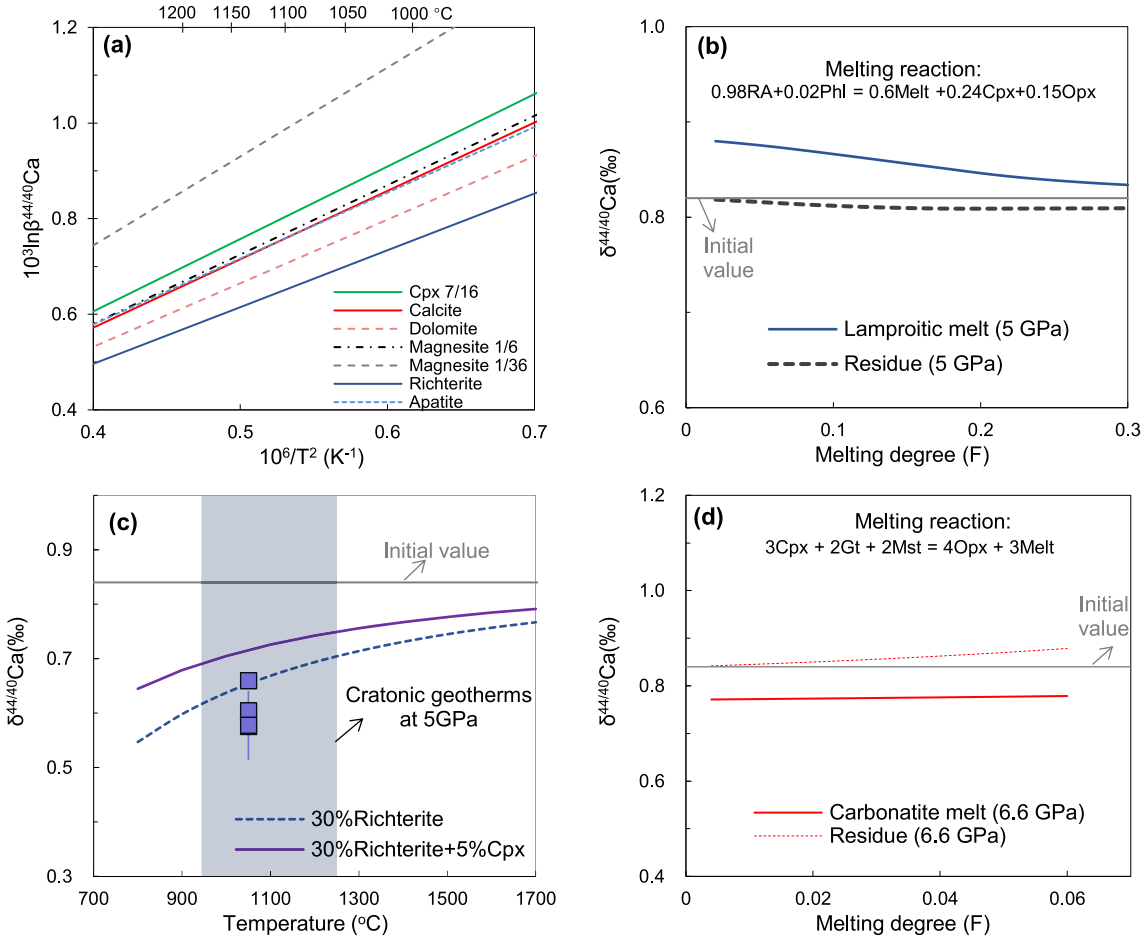

Fig. 5. (a) Calcium isotope β-factors for clinopyroxene (Ca/(Ca+Mg) = 7/16), carbonate minerals (calcite, dolomite, and magnesites with Ca/(Ca+Mg) of 1/16 and 1/36), apatite, and K-richterite from first-principles calculations (Wang et al., 2017a, 2017b; Xiao et al., 2022). (b) Modeled $\delta^{44/40}$Ca of lamproitic melts and residues with increasing degree of partial melting of MARID at 5 GPa using the melting reaction from Foley et al. (2022). The initial $\delta^{44/40}$Ca value is assumed to be the same as MORB (Chen et al., 2020a; Eriksen and Jacobsen, 2022). (c) Modeled $\delta^{44/40}$Ca of MARID (with 30 wt/% K-richterite and 30 wt/% K-richterite + 5 wt.% clinopyroxene, respectively) crystallized from silicate melt/fluid using fractionation factors in (a). The cratonic geotherms are summarized in Lee et al. (2011). (d) Modeled $\delta^{44/40}$Ca of carbonatite melts and residues with an increasing degree of partial melting of magnesite lherzolite at 6.6 GPa using the melting reaction from (Dasgupta and Hirschmann, 2007). The $\delta^{44/40}$Ca in the starting carbonated peridotite is the average value of carbonated peridotite xenoliths from the Siberian craton (Ionov et al., 2019; Zhu et al., 2021). Details of all modeling calculations are in Supplementary information: Section 3.1 and Table S3.

5.3. Calcium isotope systematics of ultramafic lamprophyres and associated carbonatites

5.3.1. Negligible calcium isotope fractionation during differentiation of carbonated silicate magma

The aillikites, mela-aillikites, damtjernites, and carbonatites studied here have identical Sr-Nd-Hf-Pb isotopic compositions, indicating that they are related to a common parental magma formed by melting of a carbonate-rich mantle domain (Tappe et al., 2006). The low SiO_2 (22.5–26.8 wt.%) and high MgO (17.3–20.9 wt.%), Ni (483–719 ppm), and Cr contents (577–734 ppm) of the aillikites testify to their near-primary nature (Tappe et al., 2006, 2008). In contrast, the mela-aillikites show higher SiO_2 (31.6–35.9 wt.%) contents but low CaO (8.2–11 wt.%) and CO_2 (2.0–5.4 wt.%) contents, falling on a trend that may correspond to the separation of a carbonate-rich component from more primitive aillikite magma, with the mela-aillikites representing the silicate-enriched portion (Fig. 6) (Tappe et al., 2006). The mela-aillikites show the same range of $\delta^{44/40}$Ca values (0.67 to 0.72 ‰) as primitive aillikites (0.71 to 0.75 ‰), indicating that separation of carbonate from silicate components, which may include decarbonation and CO_2-degassing, causes negligible fractionation of Ca isotopes.

Although the damtjernites do not lie on the same trend of carbonate liquid separation from the more primitive aillikites, they are generally SiO_2-richer (similar to the mela-aillikites) and show large variations in their SiO_2 (30.2–38 wt.%), CaO (10.3–21.2 wt.%), and CO_2 (0.2–8.1 wt.%) contents (Fig. 6 and Table S1). Damtjernites have been interpreted to result from liquid immiscibility from an alkali-rich proto-aillikite magma at relatively shallow depths (Tappe et al., 2006). Four evolved damtjernite samples with low Mg# values and high Al_2O_3 contents have slightly lower $\delta^{44/40}$Ca values (0.56 to 0.62 ‰), whereas the more primitive damtjernites show higher $\delta^{44/40}$Ca values (0.67 to 0.72 ‰). Following liquid immiscibility, these evolved damtjernites experienced fractional crystallization of olivine, clinopyroxene and apatite, as indicated by olivine phenocrysts and clinopyroxene-apatite prisms (Tappe et al., 2006). Clinopyroxene and apatite may have heavier Ca isotopes than the carbonate-bearing damtjernitic magmas, just as clinopyroxene and apatite have heavier Ca isotopes than dolomite (Fig. 5a). Therefore, fractional crystallization of clinopyroxene and apatite may induce minor Ca isotope fractionation, explaining the slightly lower $\delta^{44/40}$Ca values of the four evolved damtjernite samples. The $\delta^{44/40}$Ca values (0.67 to 0.72 ‰) of the primitive damtjernites and carbonatites (except for ST203 with a high $\delta^{44/40}$Ca value of 0.90 ‰) are similar to those of aillikites and mela-aillikites. Together, these observations suggest negligible Ca isotope fractionation during differentiation of carbonated silicate

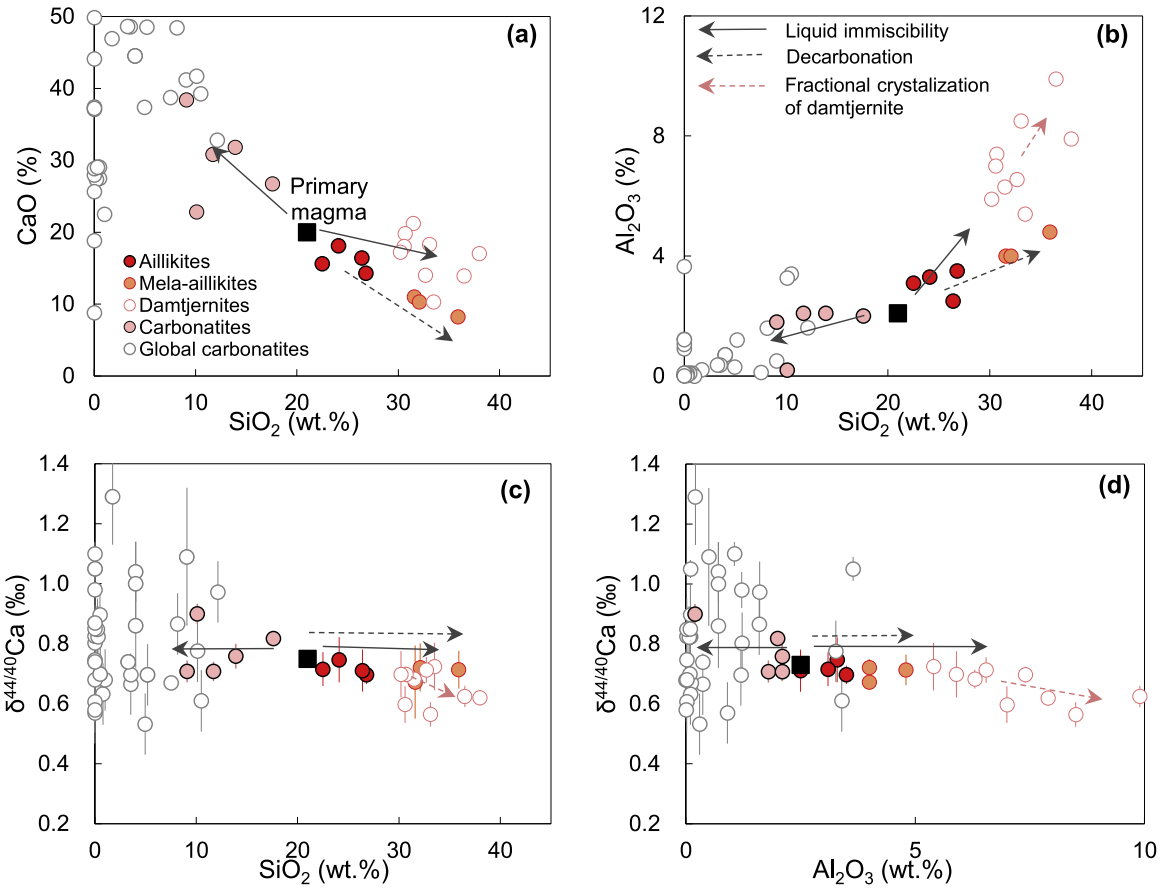

Fig. 6. Plots of SiO_2 versus CaO (a) and Al_2O_3 (b) contents and plots of $\delta^{44/40}Ca$ versus SiO_2 (c) and Al_2O_3 contents (d) for the Late Neoproterozoic ultramafic lamprophyres. Magma evolution trends (arrows) from Tappe et al. (2006). Igneous carbonatites are shown for comparison (Banerjee et al., 2021; Sun et al., 2021).

magmas including liquid immiscibility and CO_2-degassing.

5.3.2. Calcium isotope fractionation during low-degree partial melting of carbonated peridotite

The $\delta^{44/40}Ca$ values of the most primitive aillikite samples represent those of primary carbonated silicate melts (0.72 ± 0.05 ‰, 2sd) produced by incipient melting of carbonated peridotites. We compiled bulk Ca isotope compositions of carbonated peridotite xenoliths (Ionov et al., 2019; Zhu et al., 2021), which show an average $\delta^{44/40}Ca$ value of 0.82 ± 0.05 ‰, 2sd (Fig. 7a and Table S4). The significantly different $\delta^{44/40}Ca$ values for carbonated silicate melts and carbonated peridotites could potentially reflect Ca isotope fractionation during low-degree partial melting of carbonated mantle rocks. Carbonate, clinopyroxene, and garnet are the main Ca-phases in carbonated mantle peridotite domains at the pressure and temperature conditions relevant to the lowermost cratonic lithosphere and underlying convecting upper mantle. First-principles calculations can be used to predict Ca isotope fractionation between clinopyroxene and various types of carbonate minerals,

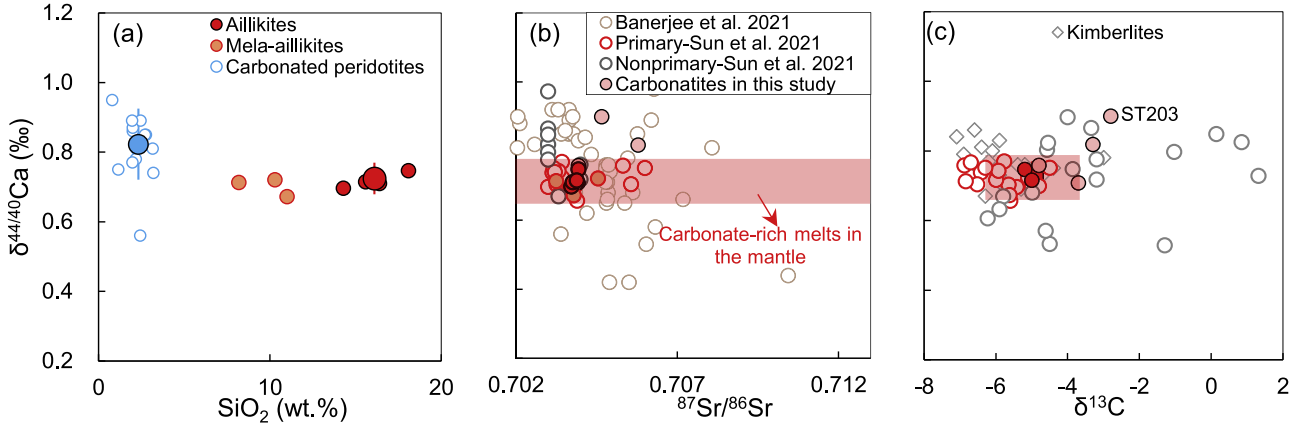

Fig. 7. (a) Comparison of $\delta^{44/40}Ca$ values of aillikites and mela-aillikites with carbonated peridotites (Table S4, Ionov et al., 2019; Zhu et al., 2021). (b-c) $\delta^{44/40}Ca$ values versus $^{87}Sr/^{86}Sr$ and $\delta^{13}C$ of carbonate-rich igneous rocks including aillikites, mela-aillikites, and carbonatites. Previously reported $\delta^{44/40}Ca$ values of global carbonatites are from Sun et al. (2021) and Banerjee et al. (2021). Sun et al. (2021) defined primary carbonatites based on their C–O isotopes (-8 ‰ $< \delta^{13}C < -4$ ‰ and 4 ‰ $< \delta^{18}O <$ 10 ‰). $\delta^{44/40}Ca$ values of kimberlites are also shown for comparison (Antonelli et al., 2023).

including calcite, dolomite, and magnesite (Wang et al., 2017a, 2017b). Results show that $\Delta^{44/40}Ca_{Carbonate\text{-}Cpx}$ is −0.04 to −0.10 when the Ca/(Mg+Ca) of the carbonate is higher than 1/6 at 1050 °C (Fig. 5a). Furthermore, garnet and Opx that are residual after low-degree melting of carbonated peridotite have heavier Ca isotope compositions than Cpx and carbonate. We quantitatively modeled the behavior of Ca isotopes during partial melting of magnesite lherzolite at 6.6 GPa using an incremental batch melting model (Chen et al., 2019; Williams and Bizimis, 2014). The inter-mineral fractionation factors for carbonate, garnet, and pyroxenes are from Chen et al. (2020b) and Wang et al. (2017a), and melting parameters are from Dasgupta et al. (2007). Details of the modeling are presented in the Supplementary Information: Section 3.1 and Table S3, and the results are illustrated in Fig. 5d. Our results show that isotope fractionation of about 0.08 ‰ $\delta^{44/40}$Ca occurs between carbonated melt and its peridotitic residue, which explains the measured differences (about 0.1 ‰) between carbonated peridotites and the carbonated silicate melts at Aillik Bay (Fig. 7a).

5.3.3. Calcium isotope compositions of carbonate-rich mantle melts

Previously reported $\delta^{44/40}$Ca values for global carbonatites show a large variation (Figs. 2 and 7). The origin of this large Ca isotope variation is unclear, and competing ideas invoke Rayleigh fractionation during late-stage precipitation of carbonates from fluid-rich carbonatite magmas (Sun et al., 2021) and the involvement of recycled sedimentary carbonate in the mantle source (Amsellem et al., 2020; Banerjee et al., 2021). The calcium isotope compositions of primitive carbonate-rich magmas from the mantle can serve as a benchmark to evaluate directions and degrees of isotope variation caused by later magmatic-hydrothermal processes or originally by mantle source contamination with recycled sedimentary carbonate components. Previous studies used the Bulk Silicate Earth (BSE) composition as the benchmark for $\delta^{44/40}$Ca (Amsellem et al., 2020; Banerjee et al., 2021). However, experiments show that melts of carbonated peridotite at >140 km depth have a carbonated silicate structure and composition (Dasgupta and Hirschmann, 2006; Pintér et al., 2021), with aillikites being the best natural analogues. Therefore, the Ca isotope compositions of the type aillikites and associated pristine carbonatites can be used to constrain the calcium isotope compositions of primitive carbonate-rich magmas in the mantle.

The average $\delta^{44/40}$Ca value of the carbonate-rich igneous rocks at Aillik Bay (aillikites and carbonatites) is 0.72 ± 0.05 ‰ (2sd, n = 11). This value is consistent with the $\delta^{44/40}$Ca of 0.72 ± 0.06 ‰ (2sd, n = 18) for pristine global carbonatites with mantle-like C–O isotope compositions (Sun et al., 2021). It is also similar to the average $\delta^{44/40}$Ca composition of magmatic kimberlites at 0.77 ± 0.11 ‰ (2sd, n = 19) (Antonelli et al., 2023). Therefore, we propose that the average value of 0.74 ‰ (2sd = 0.10 ‰; 2se = 0.02 ‰; n = 48) represents the Ca isotope composition of carbonate-rich magmas in the mantle.

Carbonatite sample ST203 from Aillik Bay has a δ^{13}C composition of −2.8 ‰ and this deviation from the mantle range (−4 to −6 ‰ δ^{13}C) was explained by high-temperature Rayleigh fractionation (Tappe et al., 2006). The high $\delta^{44/40}$Ca value of 0.90 ‰ for ST203 suggests that complex carbonatite magma evolution can fractionate the Ca and C isotope compositions, as suggested by Sun et al. (2021). This may explain the origin of high $\delta^{44/40}$Ca values in some carbonatites from occurrences worldwide (much higher than 0.72 ‰, Fig. 7b-c), which must await future detailed investigations.

5.4. Calcium isotope constraints on the metasomatic source component in the Mesozoic nephelinites

The Mesozoic nephelinites experienced fractional crystallization of olivine and clinopyroxene (see Section 5.1). The fractionation factor for Ca isotopes between clinopyroxene and silicate melt is close to 1, so that fractional crystallization of clinopyroxene does not significantly affect Ca isotopes (Chen et al., 2020a; Zhang et al., 2018). The lack of correlation between $\delta^{44/40}$Ca values and CaO/Al_2O_3 ratios also indicates that fractional crystallization of clinopyroxene did not change the Ca isotopic compositions of the nephelinites (Fig. 3b). Therefore, the $\delta^{44/40}$Ca values of the nephelinites reflect the Ca isotopic compositions of their parental magmas.

The $\delta^{44/40}$Ca values of the nephelinites are similar to those of the Late Neoproterozoic ultramafic lamprophyres and carbonatites, slightly lower than average MORB (Figs. 2 and 8). This could be attributed to either the direct effect of melting of wehrlite or to the wehrlite source already possessing low $\delta^{44/40}$Ca. Partial melting of shallow spinel-facies wehrlite (melting pressure = 2–3 GPa) cannot explain the systematically low $\delta^{44/40}$Ca values of the nephelinites relative to MORBs because the Ca budget is dominated by Cpx during partial melting (Chen et al., 2019; Zhang et al., 2018). The wehrlite-rich source of the nephelinites formed by metasomatism by carbonate-rich melts, as indicated by the low SiO_2 contents and high CaO/Al_2O_3 ratios of the nephelinites (Tappe et al., 2007). Trace element patterns of the nephelinites resemble those of aillikites, and their Sr-Nd-Hf-Pb isotope compositions indicate that their source formed by metasomatic reactions between cratonic lherzolite and aillikitic melts during the Neoproterozoic (Tappe et al., 2007). This is consistent with similar $\delta^{44/40}$Ca values for the nephelinites and the Neoproterozoic aillikites. Therefore, we suggest that the wehrlites in their mantle source already had $\delta^{44/40}$Ca values of about 0.75 ‰ as a result of metasomatism by carbonated silicate melts derived from Neoproterozoic aillikite magmatism.

5.5. A calcium isotope perspective on the composition of metasomatized cratonic mantle and the origin of alkaline magmatism

The lithosphere-asthenosphere boundary (LAB) beneath cratons represents a transition zone that undergoes episodic rejuvenation caused by the impregnation with asthenosphere-derived volatile-rich melts (Foley, 2008; O'Reilly and Griffin, 2010). The cratonic LAB is recognized as a key source of ultramafic alkaline and carbonatitic magmas, and as a zone that modulates the chemical compositions of deeper-derived magmas during their ascent (Foley et al., 2019; Giuliani et al., 2020; Tappe et al., 2023). Our results reveal that the Ca isotope compositions of metasomatized lithosphere at the base of the NAC are different from those typical for refractory cratonic mantle and the asthenosphere (Chen et al., 2019; Kang et al., 2017) (Fig. 9). For example, $\delta^{44/40}$Ca values of about 0.60 ‰ characterize the MARID-type metasomes tapped during Mesoproterozoic lamproite magmatism, and $\delta^{44/40}$Ca values of about 0.72–0.82 ‰ characterize the carbonated peridotite components that gave rise to Neoproterozoic ultramafic lamprophyre and carbonatite magmatism. Undoubtedly, the multiply metasomatically overprinted LAB beneath cratons has an important effect on the Ca isotope compositions of deep-sourced magmas (Tappe et al., 2021).

The $\delta^{44/40}$Ca values of some continental SiO_2-saturated basalts range from 0.65 to 0.80 ‰ (Liu et al., 2017), notably lower than the MORB average (Fig. 8d). This has been attributed to recycling of sedimentary carbonate into their mantle sources. However, the SiO_2-saturated nature of these basalts at low CaO/Al_2O_3 is in conflict with magma origins from a carbonated mantle source (Fig. 8). Our results for the Mesoproterozoic lamproites from the NAC indicate a key role for K-richterite in determining the Ca isotope compositions of alkaline magmas. We suggest that low-$\delta^{44/40}$Ca K-richterite in the cold metasomatized lithospheric mantle should be considered as a possible source of the low $\delta^{44/40}$Ca signature of certain SiO_2-saturated basalts. Potassic richterite is a readily fusible component enriched in Ca, Na and K, and will be an early contributor to melts generated within metasomatized lithosphere (Foley et al., 2022), but also to asthenosphere-derived melts upon their entry into metasomatized lithosphere, particularly where the lithosphere is very thick (Gao et al., 2023). The high Na_2O+K_2O contents of continental SiO_2-saturated basalts indicate that K-richterite may have been involved in producing the low $\delta^{44/40}$Ca values (Fig. 8d).

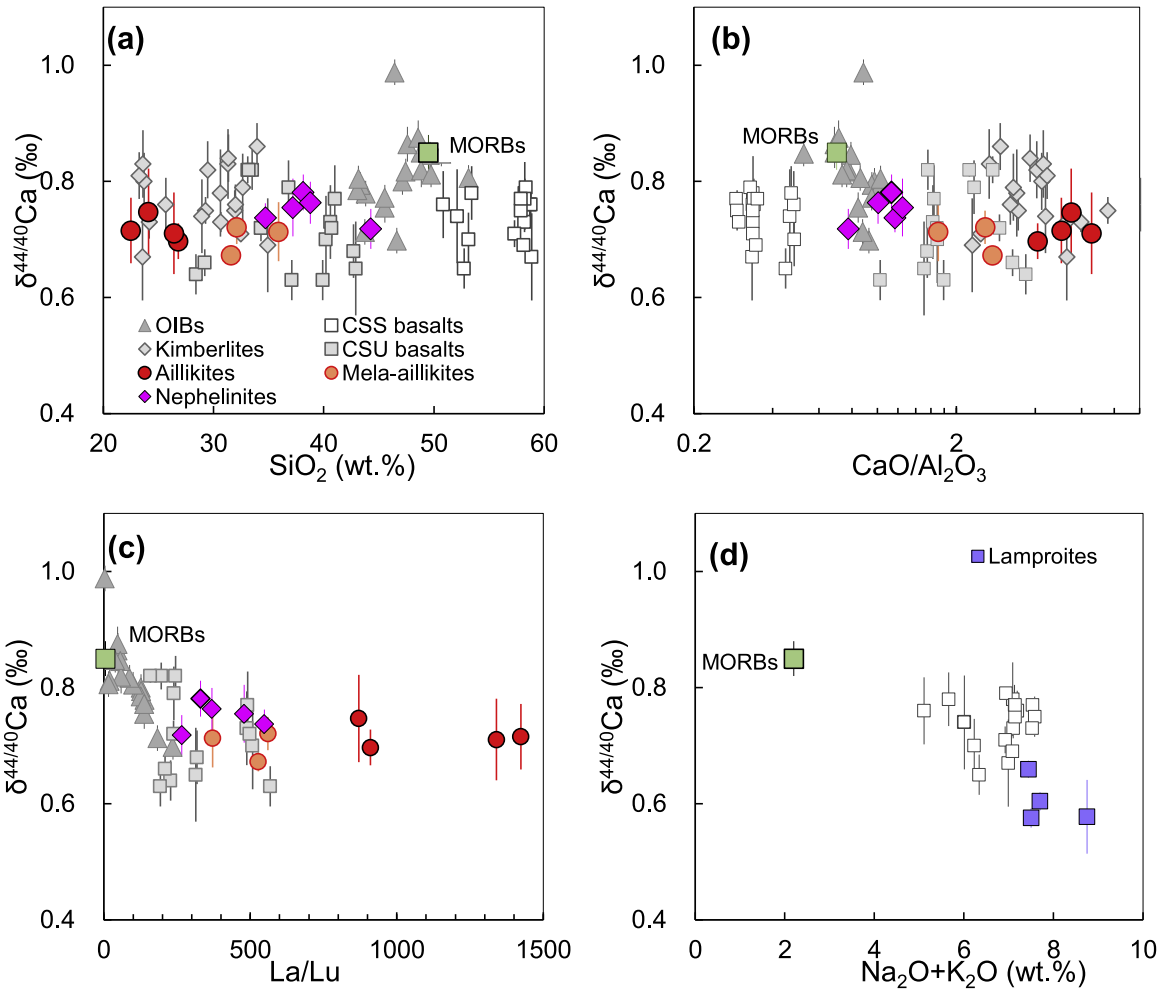

Fig. 8. Bulk rock $\delta^{44/40}$Ca versus bulk rock SiO_2 (a), CaO/Al_2O_3 (b), La/Lu ratio (c), and Na_2O+K_2O content (d) for the alkaline rocks in this study, OIBs (Eriksen and Jacobsen, 2022), continental silica-saturated (CSS basalts) (Liu et al., 2017) and silica-undersaturated (CSU basalts) alkaline basalts (Qi et al., 2022; Zhao et al., 2022), and kimberlites (Antonelli et al., 2023). Average MORB is shown for comparison (Chen et al., 2020a; Eriksen and Jacobsen, 2022; Zhu et al., 2018).

Carbonated silicate melts are stable and prevalent at >140 km depths (Dasgupta and Hirschmann, 2006) because deep mantle melting occurs only where promoted by carbon and water (Dasgupta and Hirschmann, 2006; Foley and Pintér, 2018). Our $\delta^{44/40}$Ca value of 0.74 ± 0.02 ‰ (2se) for ultramafic lamprophyres and carbonatites from a rifted craton setting serves as a benchmark for primary carbonate-rich melts in the mantle to evaluate the directions and degrees of isotope variations observed in carbonate-rich magmas, and it provides a more appropriate choice than the $\delta^{44/40}$Ca value for BSE (Chen et al., 2019; Kang et al., 2017), as used in previous studies (Banerjee et al., 2021; Qi et al., 2022; Zhao et al., 2022). Furthermore, the low $\delta^{44/40}$Ca values of the Mesozoic nephelinites from Aillik Bay suggest a role for carbonated silicate melts in the origin of SiO_2-undersaturated alkaline rocks. We suggest that the low $\delta^{44/40}$Ca values for previously reported SiO_2-undersaturated alkaline basalts (0.65 to 0.77 ‰) and some carbonatites may not trace recycled sedimentary carbonate in their mantle source as previously proposed, but rather that such Ca isotope signatures are a hallmark geochemical feature of asthenosphere-derived carbonated melts and their metasomatic products (Fig. 8). Furthermore, SiO_2-undersaturated alkaline OIBs also show lower $\delta^{44/40}$Ca values than the MORB average (Eriksen and Jacobsen, 2022; He et al., 2017; Jacobson et al., 2015; Zhang et al., 2018) (Figs. 2 and 8). The influence of carbonated silicate melts on OIB mantle sources leading potentially to low $\delta^{44/40}$Ca values should be explored in the near future.

6. Conclusions

To explore the effects of lithological mantle heterogeneity on the Ca isotope systematics of magmas, we present new Ca isotope data for lamproites, ultramafic lamprophyres, carbonatites, and nephelinites from the North Atlantic craton at Aillik Bay on the margin of the Labrador Sea rift. The Mesoproterozoic lamproites show lower $\delta^{44/40}$Ca values (0.58 to 0.66 ‰) than MORBs, suggesting an origin by melting of a MARID-type source containing K-richterite, a mineral that can cause the low-$\delta^{44/40}$Ca signature. The $\delta^{44/40}$Ca values of the Neoproterozoic ultramafic lamprophyres are relatively uniform (0.67 to 0.75 ‰) and similar to those of the carbonatites (0.71 to 0.82 ‰), discounting significant Ca isotope fractionation during liquid immiscibility of a parental carbonated silicate melt. The average $\delta^{44/40}$Ca value of the carbonate-bearing magmas is slightly, but consistently, lower than the MORB average. The $\delta^{44/40}$Ca values of the Mesozoic nephelinites (0.72 to 0.78 ‰) are similar to those of the Neoproterozoic ultramafic lamprophyres, indicating a wehrlitic metasomatic source that was formed by interaction between cratonic mantle peridotite and rising carbonated silicate magmas during the Neoproterozoic rifting stage. The new data indicate that both K-richterite and carbonate components in upper mantle environments can cause systematically low $\delta^{44/40}$Ca values in alkaline melts produced from metasomatized sources, which may explain the frequently observed low-$\delta^{44/40}$Ca signature of some intraplate continental and oceanic basalts. Our study highlights Ca isotopes

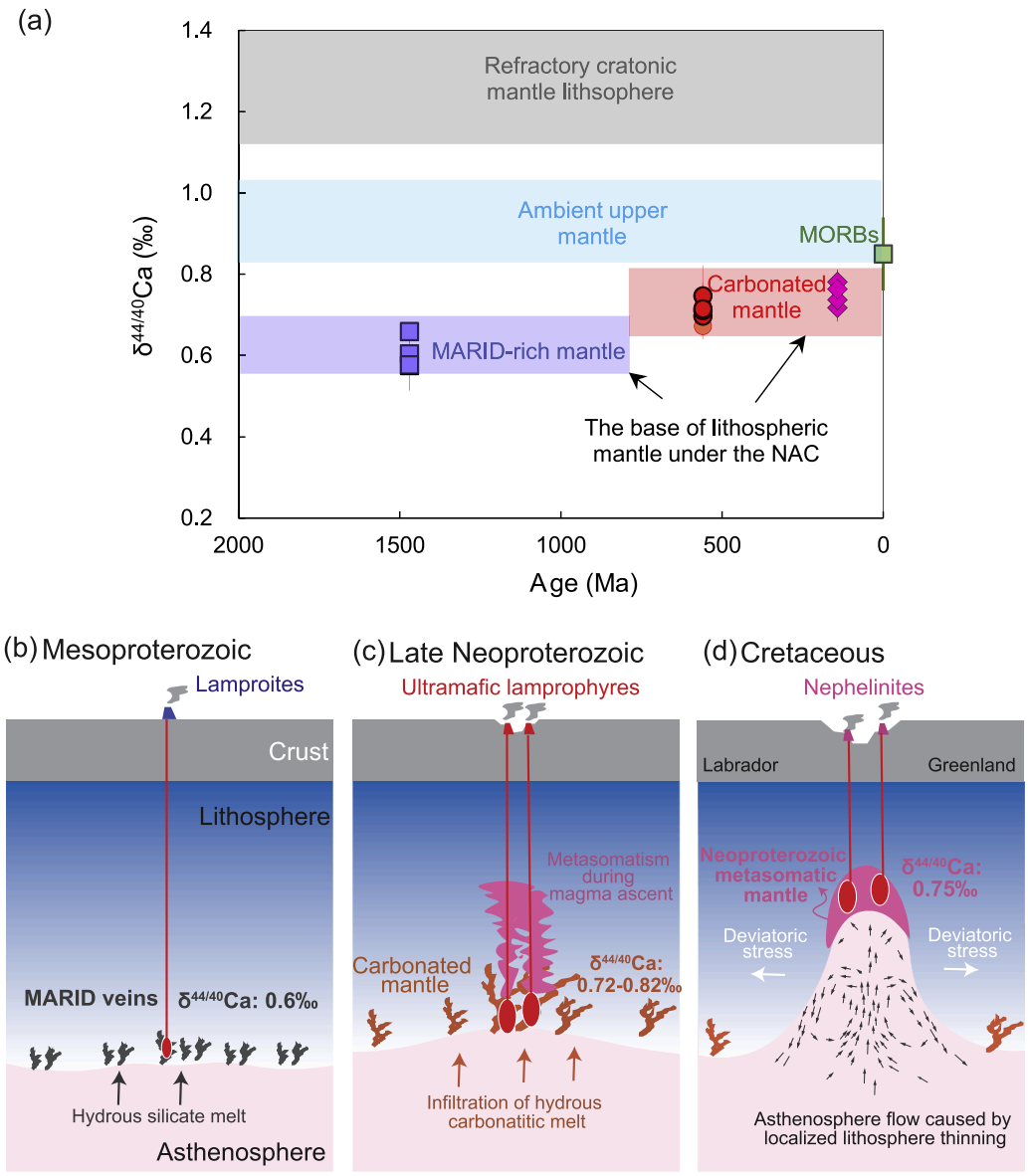

Fig. 9. Evolution of calcium isotope compositions of the metasomatic mantle lithosphere at the base of the North Atlantic craton over geological history (a-d). Calcium isotope compositions of the refractory cratonic lithospheric mantle (Chen et al., 2019; Kang et al., 2017), upper mantle (Chen et al., 2019; Kang et al., 2017), and average MORB (Chen et al., 2020a; Eriksen and Jacobsen, 2022; Zhu et al., 2018) are shown for comparison. (b-c) Schematic illustration of progressive rifting of the North Atlantic craton by episodic metasomatism and asthenospheric convection (modified after Tappe et al. (2007)). Mesoproterozoic lamproites were formed by the melting of phlogopite pyroxenite and peridotite at the base of the lithosphere in reduced conditions (b). Late Neoproterozoic ultramafic lamprophyres and carbonatites originate from the melting of phlogopite-carbonate veins derived from the solidification of carbonate-rich melts from the asthenosphere (c). The aillikitic magmas from this episode played an important role in the alteration and weakening of the shallow lithospheric mantle. The Cretaceous nephelinites were produced by melting of the lithospheric mantle (wehrlite) modified by aillikitic melt (d).

as a robust tracer of lithological variations in the mantle sources of alkaline magmas, promising to constrain the sources and mobility of volatile components within the crust-mantle system.

CRediT authorship contribution statement

Chunfei Chen: Conceptualization, Investigation, Methodology, Formal analysis, Writing – original draft. **Stephen F. Foley:** Conceptualization, Funding acquisition, Writing – review & editing. **Sebastian Tappe:** Investigation, Writing – review & editing. **Huange Ren:** Methodology, Resources. **Lanping Feng:** Methodology, Resources. **Yongsheng Liu:** Conceptualization, Funding acquisition.

Declaration of Competing Interest

The authors declare no competing interests.

Data availability

All unpublished research data used in the manuscript are included in Table 1 and supplementary tables.

Acknowledgments

This research is supported by Key R&D Program of China (2019YFA0708400), NSFC (41530211) and SKL-GPMR (MSFGPMR01).

SFF and CC are funded by ARC grant FL180100134. Mapping and sampling by ST and SFF in Labrador during 2003–2004 were financially supported by the German Research Foundation (DFG). We appreciate the constructive comments from Dr. Zack Eriksen and one anonymous reviewer that significantly improved the manuscript and Editor Rosemary Hickey-Vargas for the efficient editing of the paper. We thank Dr. Kai Wang for help with the map in Fig. 1.

Supplementary materials

Supplementary material associated with this article can be found, in the online version, at doi:10.1016/j.epsl.2023.118489.

References

Aiuppa, A., Casetta, F., Coltorti, M., Stagno, V., Tamburello, G., 2021. Carbon concentration increases with depth of melting in Earth's upper mantle. Nat. Geosci. 14, 697–703.
Amini, M., Eisenhauer, A., Böhm, F., Holmden, C., Kreissig, K., Hauff, F., Jochum, K.P., 2009. Calcium isotopes ($\delta^{44/40}$Ca) in MPI-DING reference glasses, USGS rock powders and various rocks: evidence for Ca isotope fractionation in terrestrial silicates. Geostand. Geoanal. Res. 33, 231–247.
Amsellem, E., Moynier, F., Bertrand, H., Bouyon, A., Mata, J., Tappe, S., Day, J.M., 2020. Calcium isotopic evidence for the mantle sources of carbonatites. Sci. Adv. 6, eaba3269.
Amsellem, E., Moynier, F., Pringle, E.A., Bouvier, A., Chen, H., Day, J.M.D., 2017. Testing the chondrule-rich accretion model for planetary embryos using calcium isotopes. Earth Planet. Sci. Lett. 469, 75–83.
Antonelli, M.A., Giuliani, A., Wang, Z., Wang, M., Zhou, L., Feng, L., Li, M., Zhang, Z., Liu, F., Drysdale, R.N., 2023. Subducted carbonates not required: deep mantle melting explains stable Ca isotopes in kimberlite magmas. Geochim. Cosmochim. Acta 348, 410–427.
Antonelli, M.A., Kendrick, J., Yakymchuk, C., Guitreau, M., Mittal, T., Moynier, F., 2021. Calcium isotope evidence for early Archaean carbonates and subduction of oceanic crust. Nat. Commun. 12, 2534.
Antonelli, M.A., Schiller, M., Schauble, E.A., Mittal, T., DePaolo, D.J., Chacko, T., Grew, E.S., Tripoli, B., 2019. Kinetic and equilibrium Ca isotope effects in high-T rocks and minerals. Earth Planet. Sci. Lett. 517, 71–82.
Banerjee, A., Chakrabarti, R., Simonetti, A., 2021. Temporal evolution of $\delta^{44/40}$Ca and ^{87}Sr/^{86}Sr of carbonatites: implications for crustal recycling through time. Geochim. Cosmochim. Acta 307, 168–191.
Chen, C., Ciazela, J., Li, W., Dai, W., Wang, Z., Foley, S.F., Li, M., Hu, Z., Liu, Y., 2020a. Calcium isotopic compositions of oceanic crust at various spreading rates. Geochim. Cosmochim. Acta 278, 272–288.
Chen, C., Dai, W., Wang, Z., Liu, Y., Li, M., Becker, H., Foley, S.F., 2019. Calcium isotope fractionation during magmatic processes in the upper mantle. Geochim. Cosmochim. Acta 249, 121–137.
Chen, C., Huang, J.-X., Foley, S.F., Wang, Z., Moynier, F., Liu, Y., Dai, W., Li, M., 2020b. Compositional and pressure controls on calcium and magnesium isotope fractionation in magmatic systems. Geochim. Cosmochim. Acta 290, 257–270.
Coogan, L.A., Saunders, A.D., Wilson, R.N., 2014. Aluminum-in-olivine thermometry of primitive basalts: evidence of an anomalously hot mantle source for large igneous provinces. Chem. Geol. 368, 1–10.
Dasgupta, R., 2018. Volatile-bearing partial melts beneath oceans and continents–Where, how much, and of what compositions? Am. J. Sci. 318, 141–165.
Dasgupta, R., Hirschmann, M.M., 2006. Melting in the Earth's deep upper mantle caused by carbon dioxide. Nature 440, 659–662.
Dasgupta, R., Hirschmann, M.M., 2007. Effect of variable carbonate concentration on the solidus of mantle peridotite. Am. Mineral. 92, 370–379.
Dasgupta, R., Hirschmann, M.M., Smith, N.D., 2007. Partial melting experiments of peridotite + CO_2 at 3 GPa and genesis of alkalic ocean island Basalts. J. Petrol. 48, 2093–2124.
Dawson, J.B., Smith, J.V., 1977. The MARID (mica-amphibole-rutile-ilmenite-diopside) suite of xenoliths in kimberlite. Geochim. Cosmochim. Acta 41, 309–323.
Eriksen, Z.T., Jacobsen, S.B., 2022. Calcium isotope constraints on OIB and MORB petrogenesis: the importance of melt mixing. Earth Planet. Sci. Lett. 593, 117665.
Farmer, G.L., 2014. 4.3 - Continental Basaltic Rocks. In: Holland, H.D., Turekian, K.K. (Eds.), Treatise On Geochemistry, 2nd Edition. Elsevier, Oxford, pp. 75–110.
Feng, L.-P., Zhou, L., Yang, L., DePaolo, D.J., Tong, S.-Y., Liu, Y.-S., Owens, T.L., Gao, S., 2017. Calcium isotopic compositions of sixteen USGS reference materials. Geostand. Geoanal. Res. 41, 93–106.
Feng, L., Zhou, L., Yang, L., Zhang, W., Wang, Q., Tong, S., Hu, Z., 2018. A rapid and simple single-stage method for Ca separation from geological and biological samples for isotopic analysis by MC-ICP-MS. J. Anal. At. Spectrom. 33, 413–421.
Fitzpayne, A., Giuliani, A., Hergt, J., Phillips, D., Janney, P., 2018a. New geochemical constraints on the origins of MARID and PIC rocks: implications for mantle metasomatism and mantle-derived potassic magmatism. Lithos 318-319, 478–493.
Fitzpayne, A., Giuliani, A., Phillips, D., Hergt, J., Woodhead, J.D., Farquhar, J., Fiorentini, M.L., Drysdale, R.N., Wu, N., 2018b. Kimberlite-related metasomatism recorded in MARID and PIC mantle xenoliths. Mineral. Petrol. 112, 71–84.
Foley, S., 1992. Vein-plus-wall-rock melting mechanisms in the lithosphere and the origin of potassic alkaline magmas. Lithos 28, 435–453.
Foley, S.F., 2008. Rejuvenation and erosion of the cratonic lithosphere. Nat. Geosci. 1, 503–510.
Foley, S.F., Ezad, I.S., van der Laan, S.R., Pertermann, M., 2022. Melting of hydrous pyroxenites with alkali amphiboles in the continental mantle: 1. Melting relations and major element compositions of melts. Geosci. Front. 13, 101380.
Foley, S.F., Pintér, Z., 2018. Chapter 1 - Primary Melt Compositions in the Earth's Mantle. In: Kono, Y., Sanloup, C. (Eds.), Magmas Under Pressure. Elsevier, pp. 3–42.
Foley, S.F., Prelevic, D., Rehfeldt, T., Jacob, D.E., 2013. Minor and trace elements in olivines as probes into early igneous and mantle melting processes. Earth Planet. Sci. Lett. 363, 181–191.
Foley, S.F., Yaxley, G.M., Kjarsgaard, B.A., 2019. Kimberlites from source to surface: insights from experiments. Elements 15, 393–398.
Foley, S.F., Yaxley, G.M., Rosenthal, A., Buhre, S., Kiseeva, E.S., Rapp, R.P., Jacob, D.E., 2009. The composition of near-solidus melts of peridotite in the presence of CO_2 and H_2O between 40 and 60 kbar. Lithos 112 (Supplement 1), 274–283.
Fu, H., Jacobsen, S.B., Larsen, B.T., Eriksen, Z.T., 2022. Ca-isotopes as a robust tracer of magmatic differentiation. Earth Planet. Sci. Lett. 594, 117743.
Funk, S.P., Luth, R.W., 2013. Melting phase relations of a mica–clinopyroxenite from the Milk River area, southern Alberta, Canada. Contribut. Mineral. Petrol. 166, 393–409.
Gaillard, F., Malki, M., Iacono-Marziano, G., Pichavant, M., Scaillet, B.J.S., 2008. Carbonatite melts and electrical conductivity in the asthenosphere. Science 322, 1363–1365.
Gao, M., Xu, H., Foley, S.F., Zhang, J., Wang, Y., 2023. Ultrahigh-pressure mantle metasomatism in continental collision zones recorded by post-collisional mafic rocks. GSA Bull. In press.
Giuliani, A., Pearson, D.G., Soltys, A., Dalton, H., Phillips, D., Foley, S.F., Lim, E., Goemann, K., Griffin, W.L., Mitchell, R.H., 2020. Kimberlite genesis from a common carbonate-rich primary melt modified by lithospheric mantle assimilation. Sci. Adv. 6 eaaz0424.
Green, D.H., Falloon, T.J., 1998. Pyrolite: a ringwood concept and its current expression. In: Jackson, I. (Ed.), The Earth's mantle: composition, structure, Evolution, p. 311.
Grégoire, M., Bell, D., Le Roex, A., 2002. Trace element geochemistry of phlogopite-rich mafic mantle xenoliths: their classification and their relationship to phlogopite-bearing peridotites and kimberlites revisited. Contrib. Mineral. Petrol. 142, 603–625.
Gualda, G.A.R., Ghiorso, M.S., 2015. MELTS_Excel: a Microsoft Excel-based MELTS interface for research and teaching of magma properties and evolution. Geochem. Geophys. Geosyst. 16, 315–324.
He, Y., Wang, Y., Zhu, C., Huang, S., Li, S., 2017. Mass-independent and mass-dependent ca isotopic compositions of Thirteen Geological Reference materials measured by thermal ionisation mass spectrometry. Geostand. Geoanal. Res. 41, 283–302.
Heuser, A., Schmitt, A.-D., Gussone, N., Wombacher, F., et al., 2016. Analytical methods: calcium stable isotope geochemistry. In: Gussone, N., Schmitt, A.-D., Heuser, A., Wombacher, F., Dietzel, M., Tipper, E., et al. (Eds.), Calcium Stable Isotope Geochemistry. Springer.
Ionov, D.A., Qi, Y.-H., Kang, J.-T., Golovin, A.V., Oleinikov, O.B., Zheng, W., Anbar, A.D., Zhang, Z.-F., Huang, F., 2019. Calcium isotopic signatures of carbonatite and silicate metasomatism, melt percolation and crustal recycling in the lithospheric mantle. Geochim. Cosmochim. Acta 248, 1–13.
Jacobson, A.D., Grace Andrews, M., Lehn, G.O., Holmden, C., 2015. Silicate versus carbonate weathering in Iceland: new insights from Ca isotopes. Earth Planet. Sci. Lett. 416, 132–142.
Kang, J.-T., Ionov, D.A., Liu, F., Zhang, C.-L., Golovin, A.V., Qin, L.-P., Zhang, Z.-F., Huang, F., 2017. Calcium isotopic fractionation in mantle peridotites by melting and metasomatism and Ca isotope composition of the Bulk Silicate Earth. Earth Planet. Sci. Lett. 474, 128–137.
Keen, C.E., Dickie, K., Dehler, S.A., 2012. The volcanic margins of the northern Labrador Sea: insights to the rifting process. Tectonics 31, TC1011.
Lambart, S., Laporte, D., Schiano, P., 2013. Markers of the pyroxenite contribution in the major-element compositions of oceanic basalts: review of the experimental constraints. Lithos 160-161, 14–36.
Larsen, L.M., Rex, D.C., 1992. A review of the 2500 Ma span of alkaline-ultramafic, potassic and carbonatitic magmatism in West Greenland. Lithos 28, 367–402.
Lee, C.-T.A., Luffi, P., Chin, E.J., 2011. Building and Destroying Continental Mantle. Annu. Rev. Earth Planet. Sci. 39, 59–90.
Li, Y., Wu, Z., Huang, S., Wang, W., 2022. Pressure and concentration effects on intermineral calcium isotope fractionation involving garnet. Chem. Geol. 591, 120722.
Liu, F., Li, X., Wang, G., Liu, Y., Zhu, H., Kang, J., Huang, F., Sun, W., Xia, X., Zhang, Z., 2017. Marine carbonate component in the mantle beneath the southeastern tibetan plateau: evidence from magnesium and calcium isotopes. J. Geophys. Res.: Solid Earth 122, 9729–9744.
Lloyd, F.E., Arima, M., Edgar, A.D., 1985. Partial melting of a phlogopite-clinopyroxenite nodule from south-west Uganda: an experimental study bearing on the origin of highly potassic continental rift volcanics. Contrib. Mineral. Petrol. 91, 321–329.
Malpas, J., Foley, S.F., F, K.A., 1986. Alkaline mafic and ultramafic lamprophyres from the Aillik Bay area, Labrador. Can. J. Earth Sci. 23, 1902–1918.
O'Reilly, S.Y., Griffin, W.L., 2010. The continental lithosphere–asthenosphere boundary: can we sample it? Lithos 120, 1–13.
Pearson, D.G., Canil, D., Shirey, S.B., 2003. 2.05 - mantle samples included in volcanic rocks: xenoliths and diamonds. In: Holland, H.D., Turekian, K.K. (Eds.), Treatise On Geochemistry. Pergamon, Oxford, pp. 171–275.
Pintér, Z., Foley, S.F., Yaxley, G.M., Rosenthal, A., Rapp, R.P., Lanati, A.W., Rushmer, T., 2021. Experimental investigation of the composition of incipient melts in upper mantle peridotites in the presence of CO_2 and H_2O. Lithos 396-397, 106224.

Qi, Y., Wang, Q., Wei, G.-J., Li, J., Wyman, D.A., 2022. Magnesium and calcium isotopic geochemistry of silica-undersaturated alkaline basalts: applications for tracing recycled carbon. Geochem. Geophys. Geosyst. 23, e2022GC010463.
Rock, N.M.S., 1986. The nature and origin of ultramafic lamprophyres: alnöites and allied rocks. J. Petrol. 27, 155–196.
Schiller, M., Paton, C., Bizzarro, M., 2012. Calcium isotope measurement by combined HR-MC-ICPMS and TIMS. J. Anal. At. Spectrom. 27, 38–49.
Smart, K.A., Tappe, S., Ishikawa, A., Pfänder, J.A., Stracke, A., 2019. K-rich hydrous mantle lithosphere beneath the Ontong Java Plateau: significance for the genesis of oceanic basalts and Archean continents. Geochim. Cosmochim. Acta 248, 311–342.
Stagno, V., Frost, D.J., 2010. Carbon speciation in the asthenosphere: experimental measurements of the redox conditions at which carbonate-bearing melts coexist with graphite or diamond in peridotite assemblages. Earth Planet. Sci. Lett. 300, 72–84.
Sun, C., Dasgupta, R., 2020. Thermobarometry of CO2-rich, silica-undersaturated melts constrains cratonic lithosphere thinning through time in areas of kimberlitic magmatism. Earth Planet. Sci. Lett. 550, 116549.
Sun, J., Zhu, X., Belshaw, N., Chen, W., Doroshkevich, A., Luo, W., Song, W., Chen, B., Cheng, Z., Li, Z., 2021. Ca isotope systematics of carbonatites: insights into carbonatite source and evolution. Geochem. Perspect. Lett. 17, 11–15.
Tappe, S., Foley, S.F., Jenner, G.A., Heaman, L.M., Kjarsgaard, B.A., Romer, R.L., Stracke, A., Joyce, N., Hoefs, J., 2006. Genesis of ultramafic lamprophyres and carbonatites at Aillik Bay, Labrador: a consequence of incipient lithospheric thinning beneath the North Atlantic Craton. J. Petrol. 47, 1261–1315.
Tappe, S., Foley, S.F., Jenner, G.A., Kjarsgaard, B.A., 2005. Integrating ultramafic lamprophyres into the IUGS classification of igneous rocks: rationale and implications. J. Petrol. 46, 1893–1900.
Tappe, S., Foley, S.F., Kjarsgaard, B.A., Romer, R.L., Heaman, L.M., Stracke, A., Jenner, G.A., 2008. Between carbonatite and lamproite—Diamondiferous Torngat ultramafic lamprophyres formed by carbonate-fluxed melting of cratonic MARID-type metasomes. Geochim. Cosmochim. Acta 72, 3258–3286.
Tappe, S., Foley, S.F., Stracke, A., Romer, R.L., Kjarsgaard, B.A., Heaman, L.M., Joyce, N., 2007. Craton reactivation on the Labrador Sea margins: 40Ar/39Ar age and Sr–Nd–Hf–Pb isotope constraints from alkaline and carbonatite intrusives. Earth Planet. Sci. Lett. 256, 433–454.
Tappe, S., Massuyeau, M., Smart, K.A., Woodland, A.B., Gussone, N., Milne, S., Stracke, A., 2021. Sheared peridotite and megacryst formation beneath the kaapvaal craton: a snapshot of tectonomagmatic processes across the lithosphere–asthenosphere transition. J. Petrol. 62, 1–39.
Tappe, S., Ngwenya, N.S., Stracke, A., Romer, R.L., Glodny, J., Schmitt, A.K., 2023. Plume–lithosphere interactions and LIP-triggered climate crises constrained by the origin of Karoo lamproites. Geochim. Cosmochim. Acta 350, 87–105.
Tappe, S., Romer, R.L., Stracke, A., Steenfelt, A., Smart, K.A., Muehlenbachs, K., Torsvik, T.H., 2017. Sources and mobility of carbonate melts beneath cratons, with implications for deep carbon cycling, metasomatism and rift initiation. Earth Planet. Sci. Lett. 466, 152–167.
Valdes, M.C., Moreira, M., Foriel, J., Moynier, F., 2014. The nature of Earth's building blocks as revealed by calcium isotopes. Earth Planet. Sci. Lett. 394, 135–145.
Veter, M., Foley, S.F., Mertz-Kraus, R., Groschopf, N., 2017. Trace elements in olivine of ultramafic lamprophyres controlled by phlogopite-rich mineral assemblages in the mantle source. Lithos 292-293, 81–95.
Wang, W., Qin, T., Zhou, C., Huang, S., Wu, Z., Huang, F., 2017a. Concentration effect on equilibrium fractionation of Mg-Ca isotopes in carbonate minerals: insights from first-principles calculations. Geochim. Cosmochim. Acta 208, 185–197.
Wang, W., Zhou, C., Qin, T., Kang, J.-T., Huang, S., Wu, Z., Huang, F., 2017b. Effect of Ca content on equilibrium Ca isotope fractionation between orthopyroxene and clinopyroxene. Geochim. Cosmochim. Acta 219, 44–56.
Wang, Y., He, Y., Wu, H., Zhu, C., Huang, S., Huang, J., 2019. Calcium isotope fractionation during crustal melting and magma differentiation: granitoid and mineral-pair perspectives. Geochim. Cosmochim. Acta 259, 37–52.
Wardle, R.J., Hall, J., 2002. Proterozoic evolution of the northeastern Canadian Shield: lithoprobe Eastern Canadian Shield Onshore–Offshore Transect (ECSOOT), introduction and summary. Can. J. Earth Sci. 39, 563–567.
Williams, H.M., Bizimis, M., 2014. Iron isotope tracing of mantle heterogeneity within the source regions of oceanic basalts. Earth Planet. Sci. Lett. 404, 396–407.
Windley, B.F., Garde, A.A., 2009. Arc-generated blocks with crustal sections in the North Atlantic craton of West Greenland: crustal growth in the Archean with modern analogues. Earth Sci. Rev. 93, 1–30.
Xiao, Z., Zhou, C., Kang, J., Wu, Z., Huang, F., 2022. The factors controlling equilibrium inter-mineral Ca isotope fractionation: insights from first-principles calculations. Geochim. Cosmochim. Acta 333, 373–389.
Yang, Z.-F., Li, J., Liang, W.-F., Luo, Z.-H., 2016. On the chemical markers of pyroxenite contributions in continental basalts in Eastern China: implications for source lithology and the origin of basalts. Earth Sci. Rev. 157, 18–31.
Yuan, H., French, S., Cupillard, P., Romanowicz, B., 2014. Lithospheric expression of geological units in central and eastern North America from full waveform tomography. Earth Planet. Sci. Lett. 402, 176–186.
Zhang, H., Wang, Y., He, Y., Teng, F.-Z., Jacobsen, S.B., Helz, R.T., Marsh, B.D., Huang, S., 2018. No Measurable Calcium Isotopic Fractionation During Crystallization of Kilauea Iki Lava Lake. Geochem. Geophys. Geosyst. 19, 3128–3139.
Zhao, K., Dai, L.-Q., Fang, W., Zheng, Y.-F., Zhao, Z.-F., Zheng, F., 2022. Decoupling between Mg and Ca isotopes in alkali basalts: implications for geochemical differentiation of subduction zone fluids. Chem. Geol. 606, 120983.
Zhu, H., Ionov, D.A., Du, L., Zhang, Z., Sun, W., 2021. Ca-Sr isotope and chemical evidence for distinct sources of carbonatite and silicate mantle metasomatism. Geochim. Cosmochim. Acta 312, 158–179.
Zhu, H., Liu, F., Li, X., Wang, G., Zhang, Z., Sun, W., 2018. Calcium isotopic compositions of normal mid-ocean ridge basalts from the Southern Juan de Fuca Ridge. J. Geophys. Res.: Solid Earth 123, 1303–1313.